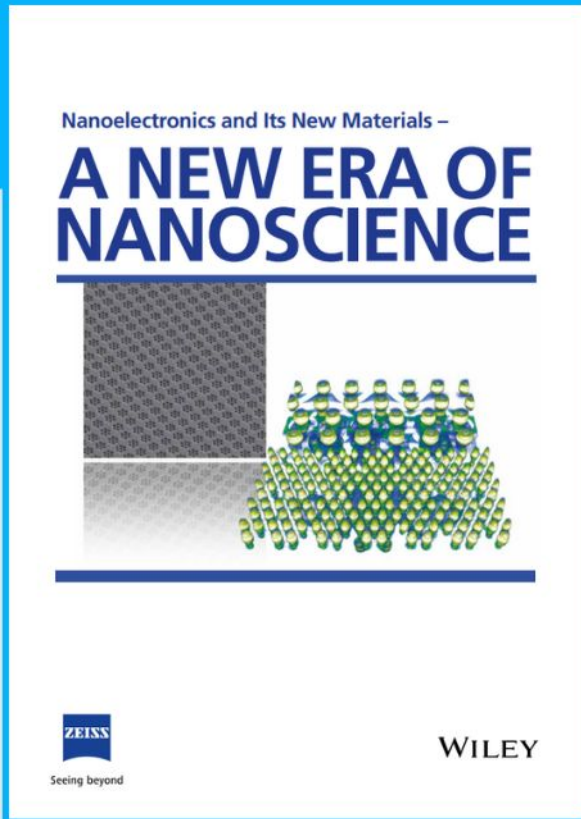




Nanoelectronics and Its New Materials – A NEW ERA OF NANOSCIENCE



Discover the recent advances in electronics research and fundamental nanoscience.

Nanotechnology has become the driving force behind breakthroughs in engineering, materials science, physics, chemistry, and biological sciences. In this compendium, we delve into a wide range of novel applications that highlight recent advances in electronics research and fundamental nanoscience. From surface analysis and defect detection to tailored optical functionality and transparent nanowire electrodes, this eBook covers key topics that will revolutionize the future of electronics.

To get your hands on this valuable resource and unleash the power of nanotechnology, simply download the eBook now. Stay ahead of the curve and embrace the future of electronics with nanoscience as your guide.



Seeing beyond

WILEY

3D Printing of Small-Scale Soft Robots with Programmable Magnetization

Mohammad Hasan Dad Ansari,* Veronica Iacovacci, Stefano Pane, Mouloud Ourak, Gianni Borghesan, Izadyar Tamadon, Emmanuel Vander Poorten, and Arianna Menciassi

Soft magnetic structures having a non-uniform magnetization profile can achieve multimodal locomotion that is helpful to operate in confined spaces. However, incorporating such magnetic anisotropy into their body is not straightforward. Existing methods are either limited in the anisotropic profiles they can achieve or too cumbersome and time-consuming to produce. Herein, a 3D printing method allowing to incorporate magnetic anisotropy directly into the printed soft structure is demonstrated. This offers at the same time a simple and time-efficient magnetic soft robot prototyping strategy. The proposed process involves orienting the magnetized particles in the magnetic ink used in the 3D printer by a custom electromagnetic coil system acting onto the particles while printing. The resulting structures are extensively characterized to confirm the validity of the process. The extent of orientation is determined to be between 92% and 99%. A few examples of remotely actuated small-scale soft robots that are printed through this method are also demonstrated. Just like 3D printing gives the freedom to print a large number of variations in shapes, the proposed method also gives the freedom to incorporate an extensive range of magnetic anisotropies.

1. Introduction

Soft materials have proven their impact in diverse fields such as flexible electronics,^[1] soft robotics,^[2] and biomedicine.^[3] In light of their ability to easily deform and adapt to the environment, soft materials can provide functionalities beyond traditional ones when developing novel actuators.^[4] These features are particularly attractive when targeting medical applications, thanks to the inherent safety of soft materials in interacting with body tissues.^[5] Soft materials exist that can be triggered to undergo shape transformation and perform actuation tasks in response to a wide range of stimuli, such as heat,^[6] light,^[7] chemicals,^[8] pressure,^[9] or magnetic fields.^[10] Out of these stimuli, magnetic triggering and actuation are especially promising due to their wireless nature, safe interaction with tissues, and miniaturization potential.^[11] Combining the

advantages offered by magnetic actuation and soft materials is therefore an attractive direction for the next generation of devices operating in demanding applications, such as medical instruments.^[5]

Small-scale robots refer to miniature robotic systems, including centimeter-sized devices down to devices with dimensions at millimeter scale.^[12] Small-scale, magnetic-responsive soft robots typically owe their magnetization to discrete magnets included in soft materials,^[13] or to thin metallic layer coatings.^[14] As an alternative, soft elastomers or hydrogels and magnetic particle composites can act as constitutive materials for soft magnetic robots.^[15] However, such approaches only allow to obtain uniform magnetization profiles, i.e., along a single preferential direction or dependent on the externally applied magnetic field.^[10a] Isotropic magnetization limits the number of possible degrees of freedom, prevents selective actuation of one portion of the robot, as well as articulated actuation and shape profiles.

Recently, methods that allow incorporating magnetic anisotropy in soft robots have been proposed.^[16] These methods can be grouped into two categories: methods incorporating anisotropy i) after the soft robot has been fabricated, or ii) while fabricating the soft robot. The starting material is the same for both the categories, i.e., a magnetic composite of a soft resin and magnetic particles. In the first category, the soft robots are fabricated through traditional procedures, such as molding,


M. H. D. Ansari, V. Iacovacci, S. Pane, A. Menciassi
The BioRobotics Institute
Scuola Superiore Sant'Anna
Via Rinaldo Piaggio 34, 56025 Pontedera, Italy
E-mail: hasan.mohammad@santannapisa.it

M. H. D. Ansari, V. Iacovacci, S. Pane, A. Menciassi
Department of Excellence in Robotics & AI
Scuola Superiore Sant'Anna
Via Rinaldo Piaggio 34, 56025 Pontedera, Italy

M. H. D. Ansari, M. Ourak, G. Borghesan, E. Vander Poorten
Department of Mechanical Engineering
KU Leuven
3000 Leuven, Belgium

G. Borghesan
Core lab Rob
Flanders Make
3000 Leuven, Belgium

I. Tamadon
Department of Biomedical Engineering
University of Twente
7522 NB Enschede, Netherlands

 The ORCID identification number(s) for the author(s) of this article can be found under <https://doi.org/10.1002/adfm.202211918>.

© 2023 The Authors. Advanced Functional Materials published by Wiley-VCH GmbH. This is an open access article under the terms of the Creative Commons Attribution-NonCommercial License, which permits use, distribution and reproduction in any medium, provided the original work is properly cited and is not used for commercial purposes.

DOI: 10.1002/adfm.202211918

and then magnetized using dedicated jigs steering the desired magnetization profile.^[10b,16a] While this method is advantageous due to its simplicity and repeatability, it is limited in shape of the soft robot, the discrete nature of the magnetization, and is further highly jig/mold dependent. This implies programming a priori the robot based on the desired shape change to be triggered. 3D printing features a great potential to overcome this limitation, as it allows to manufacture novel designs that were previously unachievable.^[17] The second category of methods to incorporate anisotropy works at the level of the fabrication process, usually by using a 3D printer for material extrusion and a magnetic field source to orient the composite particles while being extruded.^[16d] This method is advantageous in quickly producing 3D structures with anisotropies. However, the range of anisotropies that can be generated following this approach is still limited to 2D directions. This is because the methods proposed so far only allow orienting the particles along the printing direction.^[16d] A special case of this category of fabrication is reported in ^[16e] where microscale building blocks, called voxels, are assembled to produce the final robot. Each voxel is magnetized in a specific direction such that the assembled robot can have an overall magnetic anisotropy. While this method is not limited in terms of the magnetic anisotropy it can result in, it becomes increasingly difficult and time-consuming to build complex 3D structures through the assembly of microscale voxels. Therefore, both categories are specific in terms of magnetization directions they can achieve efficiently.

Table 1 provides a summary of the state-of-the-art fabrication methods along with their features. As evident in Table 1 and as mentioned in the literature, a robust 3D printing process that allows producing structures with omnidirectional 3D magnetization profiles is still lacking.^[20] To fill this gap, this paper proposes a method to print soft magnetic robots based on elastomeric magnetic composites with arbitrary programmable

magnetization profiles. To this aim, a custom set-up including an extrusion-based 3D printer, a UV light source for curing, and a dedicated electromagnetic coils system for particles orientation was developed. The new approach also overcomes the need to have unique custom jigs for specific magnetization profiles. The desired magnetization is obtained by orienting already-magnetized particles in the desired directions. This approach requires much lower currents in the electromagnetic system than the ones required to magnetize the particles from the scratch. The resulting magnetization is in the direction of the magnetic moment of the particles.

Filaments with magnetization along three mutually perpendicular directions were printed and magnetically characterized to assess the capability of this method to produce on-demand preferential magnetization. In order to prove the suitability of the method for small-scale soft robots prototyping, three designs were identified as case studies. The designs are based on different magnetization profiles to target different actuation tasks. Successful experiments with these robot designs show the value and potentialities of the proposed custom 3D printing system.

2. Results and Discussion

The printing process is schematized in **Figure 1**. The process starts with preparation of the composite magnetic ink. Neodymium Iron Boron (NdFeB) particles, 5 μm in size, are used as magnetic doping agents in light of their high remanence at room temperature.^[20] This property not only helps in imparting higher residual magnetization strength to the printed materials but also helps in the orientation process. A high viscosity (70 Pa s) UV-curable resin was selected as the ink elastomer. While on the one hand higher viscosity necessitates a higher

Table 1. Summary of state-of-the-art fabrication methods to incorporate magnetic anisotropy. A template, mold or jig is required by some fabrication methods to assist in the magnetization procedure. The degrees of freedom of magnetization refer to the potential to obtain a magnetization in any arbitrary direction anywhere in the structure. The shape of the structure refers to the dimensionality of the demonstrated structures which are mostly 2D or 3D. The scale of the process refers to the size of the structures that were presented in these works.

Reference	Method to incorporate anisotropy	Material	Jig/mold required?	Degrees of freedom of magnetization	Shape of structure	Scale
Song et.al. ^[16c]	Multi-directional planar orientation while Inkjet printing	Aqueous suspension of Co-based nanoparticles	No	2	2D	cm
Kim et.al. ^[18]	Orientation of particles in resin while curing in molds	Photocurable polymer and magnetic nanoparticles	Yes	3	2D	μm to mm
Xu et.al. ^[16b]	Orientation of particles in resin while curing in molds	UV-curable elastomer and magnetic microparticles	Yes	3	3D	mm to cm
Hu et.al. ^[16a]	Jig-assisted post-curing magnetization	Heat-curable silicone elastomer and magnetic microparticles	Yes	3	2D	mm to cm
Deng et.al. ^[19]	Laser – induced particle reorientation in cured composites	Silicone elastomer and Polycaprolactone-coated magnetic microparticles	No	3	2D	mm to cm
Kim et.al. ^[16d]	Unidirectional orientation while 3D printing	Heat-curable silicone Elastomer and magnetic microparticles	No	1	3D	mm to cm
Zhang et.al. ^[16e]	Manual assembly of directional voxels	Various soft polymers and magnetic microparticles	Yes	3	3D	μm to mm
This work	Omnidirectional orientation while 3D printing	UV-curable ink and magnetic microparticles	No	3	2D	mm to cm

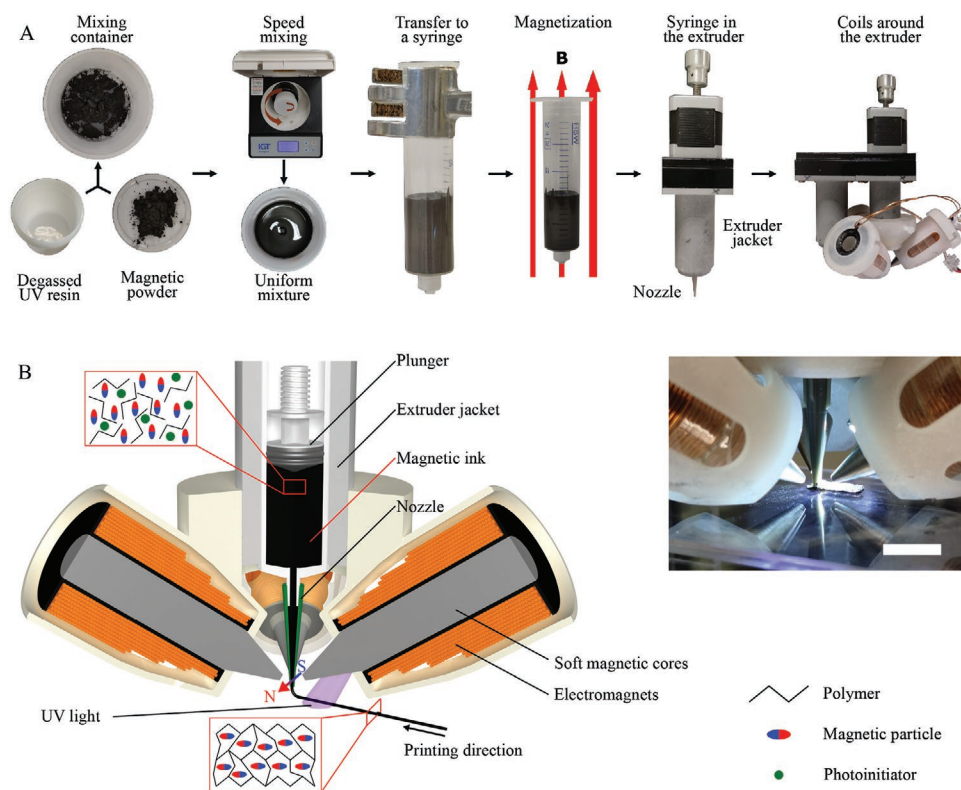


Figure 1. Small-scale soft robots with programmable magnetization fabrication process overview. A) The process for preparing the ink starts with planetary mixing the magnetic particles and the degassed UV-curable resin. The mixture was transferred to a syringe and magnetized to produce the magnetic ink. The syringe was placed in the custom extrusion system with a motorized extruder and a three Electromagnetic (EM) coil system around it. B) A schematization of the custom magnetic printing process. The magnetic particles were oriented due to the magnetic field produced by the three EM coil system. A section view of the EM system also shows the coils and cores used. The inset shows the actual fabrication procedure in action. Scale bar: 1 cm.

extrusion pressure, on the other hand it helps in keeping the shape of the printed objects during curing. The resin, photoinitiator, and magnetic microparticles were mixed and the resulting uniform mixture was magnetized resulting in the printable magnetic ink. This ink was extruded through a nozzle that has three mutually orthogonal Electromagnetic (EM) coils placed symmetrically around it such that the nozzle is at the same angle of 54.74° from each coil. As the magnetic ink was extruded, the coils oriented the magnetized particles in the desired direction at the extrusion point. By pre-calculating the currents in each coil, the magnetic field was tuned in direction and strength at the extrusion point. This aligned the magnetic particles embedded in the extruded material along the magnetic field. After extrusion, the material was UV-cured thereby locking the shape of the structure, and the orientation of the magnetic particles within it. The resulting magnetization in the structure was along the direction of the magnetic moment of the particles. The time taken for the particles to be oriented along the applied magnetic fields was also theoretically calculated following an analysis similar to the one reported by Liu et al. and as described in the Experimental Section.^[21] With this information, an upper limit on the printing speed was determined to be 300 mm min^{-1} . The orientation dynamics of magnetic particles in an external magnetic field are explained in Supporting Information and in Figure S1 (Supporting Information).

When the magnetic ink was extruded without running any current in the coils, the particles in the extruded material were oriented along the printing direction due to the magnetization step described in the Experimental Section and shown in Figure 1A. This biased direction, which coincides with the printing direction, is henceforth referred to as direction X.

The arrangement of the electromagnetic (EM) coils is shown in Figure 1B. EM coils were preferred over permanent magnets as they can produce time- and intensity-varying magnetic fields without involving any physical movement of the magnetic field source (as it would be needed in the case of permanent magnets). Furthermore, their intensity can be precisely tuned/regulated simply by controlling the currents in the coils. EM coils can also be turned off when required to produce no fields; something that cannot be done with permanent magnets. The number of coils included in the EM-based particle orientation setup was selected as a compromise between space constraints and the range of orientation directions achievable in the printing process. The constrained space available around the extrusion system nozzle limits the number of coils that can be placed around it. To produce a net magnetic field in any arbitrary direction at the extrusion point leading to 3 degrees of freedom for particle orientation, at least 3 coils are needed. Each of the 3 coils is orthogonal to the other two and was positioned symmetrically around the nozzle. The net magnetic field

produced at the extrusion point was the vector sum of the magnetic fields produced by the three coils. By controlling the magnitude of magnetic field vector from each coil independently, the net magnetic field at the extrusion point can vary in any arbitrary direction.

Model-based dimensioning was performed for coils design. Given the symmetry of the system, a single coil was modelled through Finite-Element analysis (COMSOL Multiphysics® 5.2) to derive magnetic field spatial distribution when varying coil driving current up to 3A. Higher currents run the risk of overheating the coils and damaging them. The magnetic field produced increased with an increase in the number of windings in the coil. Therefore, considering spatial constraints a stepped design was chosen to maximize the number of windings that can be accommodated in the coil (Figure 2). The simulation results in Figure 2B confirmed that the tapered cores were able to carry and concentrate the field along the core axis. It can also be seen that the field strength reduced drastically with distance from the core (Figure 2C), implying the need to have the cores close to the extrusion point. However, due to space constraints the only way to bring the cores closer to the extrusion point was by tapering them. Considering this fact, the tapered core extremities were placed 5 mm far from the extrusion point. Reducing the distance further might increase the magnitude of the field produced at the extrusion point, thus easing the

orientation process. However, this also increases the magnitude of field gradients which tend to attract the extruded ink toward one of the coils. Therefore, this distance was chosen as a compromise between the two effects. Magnetic field strength increased linearly with the current in the coils and no saturation was observed with driving currents up to 3A (Figure 2D). Each coil was also tested for its response time, as a slow response time will introduce a lag between the produced field and the required field. A fast response time ensures that the particles are oriented in the right direction at the right printing coordinates. The experimental dynamic response of a single coil is shown in Figure 2E. A step input with a step of 1 A current was supplied to each coil and the resulting magnetic field was recorded. It can be observed that as the step current is given, the field also increased and stabilized to a higher value within a few milliseconds, which is a good response time when considering the extrusion and curing dynamics (Supporting Information) and the printing speed (25 mm min^{-1}).

Employing the printing method as described above and shown in Figure 1, several sample filaments were extruded (Figure 1B). The particles were oriented such that, employing the 3 degrees of freedom of orientation, the final magnetization was along one of the six fundamental directions – direction X (aligned with direction of printing, as described earlier), the two perpendicular directions (Y and Z) with respect to X (Figure 3),

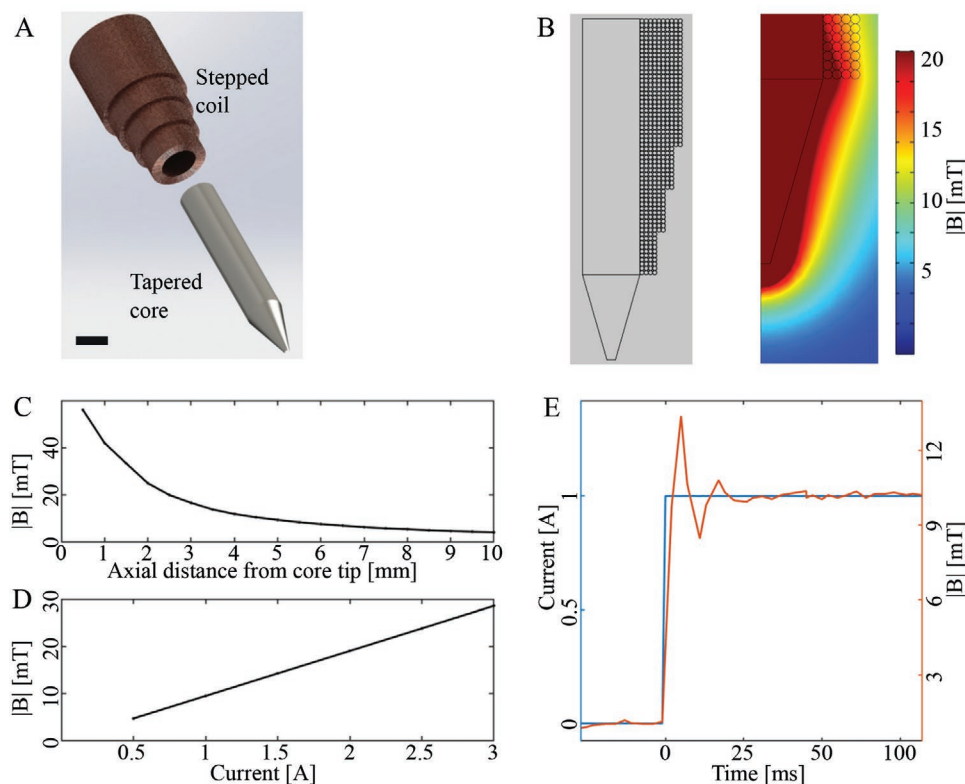


Figure 2. Single coil modelling and characterization results. A) Exploded view of the 3D CAD model of one of the coils showing the stepped coil windings and the tapered core. Scale bar: 10 mm. B) The geometric model used for COMSOL® simulation is shown where the field intensity can be seen around one coil. C) The magnetic field intensity along the axis of one of the coils with respect to the distance from the core tip with 1 A current running in the coil as calculated through modelling. D) The magnetic field intensity along the axis of the coil with respect to the current flowing in the windings at the extrusion point (5 mm distance from the core tip) as calculated through modelling. E) Experimentally measured response of one of the coils to a step-input in current is shown, confirming a fast response time ($\approx 20 \text{ ms}$).

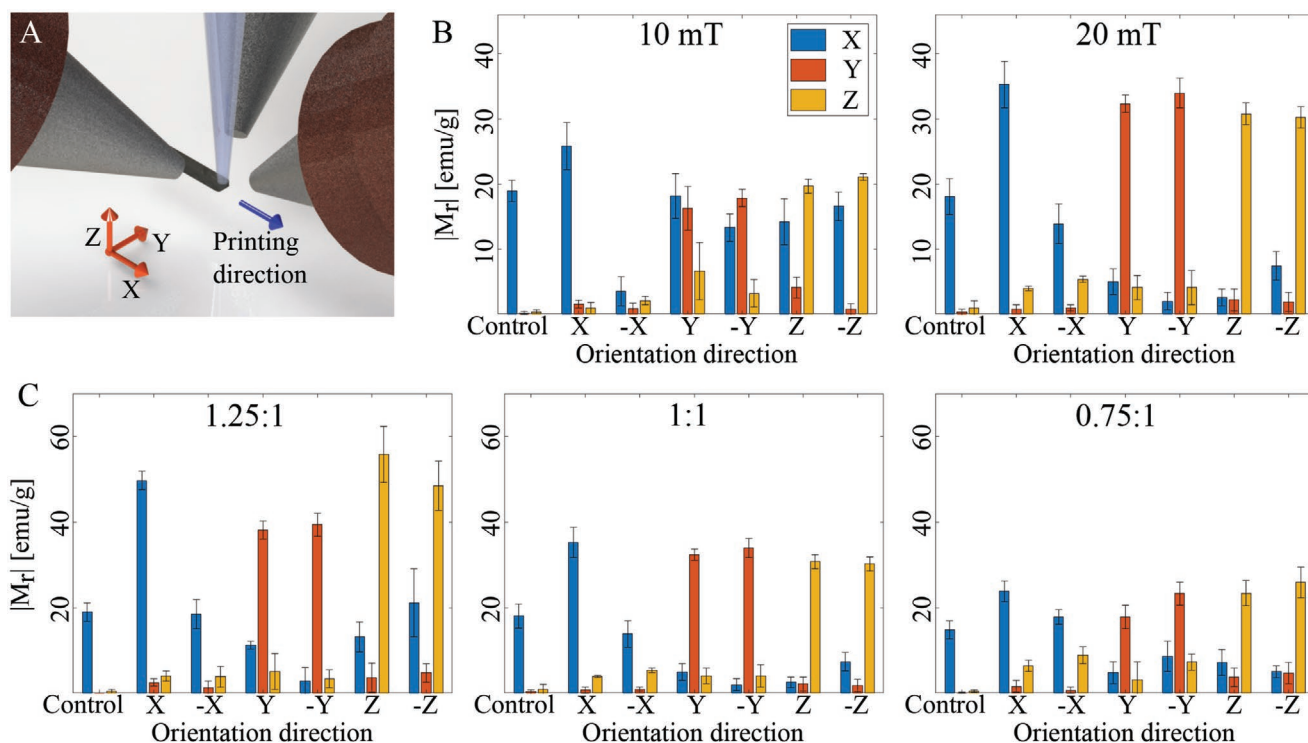


Figure 3. Selective directional magnetization characterization. A) The three mutually orthogonal directions (X, Y, and Z) in the printed material along which the particles were oriented in the printed filaments. B) The effect of field strength on resultant magnetization. The concentration of particles was 1:1 by weight with respect to the resin. C) The effect of particle concentration on the resultant magnetization. The ratios were the concentration of magnetic particles with respect to the resin by weight in the magnetic ink. The magnetic field employed was 20 mT. All means and standard deviations are for 5 samples.

and the respective opposite directions (-X, -Y, and -Z). Due to the printing process, the extruded material including the particles rotate by 90° about the Y-axis when deposited on the printing bed. Since the orientation due to magnetic field happens before the material is deposited on the printing bed, this rotation of material had to be compensated for when calculating the magnetic field to be produced. To achieve magnetization in the X-direction, magnetic field must be produced in the Z-direction. Similarly, to achieve magnetization in the Z-direction, magnetic field must be produced in the -X-direction, and to achieve magnetization in the Y-direction, magnetic field must be produced in the Y-direction, and so on. The extruded filaments were characterized in a Vibrating Sample Magnetometer (VSM) to quantify their magnetization and to understand if the approach of orienting particles in the pre-magnetized ink was feasible. The extent of orientation was measured in terms of the preferential magnetization index which is defined in Equation 1.

$$\text{preferential magnetization index} = \frac{|\text{magnetization in the preferential direction}|}{|\text{total magnetization}|} \quad (1)$$

It can be observed that the preferential magnetization index will always lie between 0 and 1. The effect of field strength on the orientation process was studied by printing filaments with magnetization in the six directions while varying the field strength (10 and 20 mT, Figure 3B). A high preferential

magnetization index (0.99) is observed in the X direction with both 10 and 20 mT fields as that is the biased direction. Barring that, 10 mT field produced preferential magnetization indices between 0.63 and 0.80, and 20 mT field produced preferential magnetization indices between 0.92 and 0.99. It can be inferred that 10 mT field is not enough to overcome the bias in the ink which leads to a lower index (lower than 0.80) in all non-bias directions. However, while the index is high in all the directions with 20 mT field, it is the lowest in the -X-direction as the particles had to be rotated by 180° while for other directions the particles had to be rotated by 90° . Nonetheless, higher preferential magnetization indices when applying 20 mT field lead to the conclusion that 20 mT field can better orient the particles while printing and this value was used in all further experiments. Increasing the magnetic field further could help with achieving a good preferential magnetization index. However, that was not done because of two reasons. First, increasing the magnetic field requires increasing the currents in the coils

which could result in overheating and damage to them. Second, an increase in the magnetic field also leads to an increase in the magnetic field gradients which tend to attract the extruded materials toward the coils, which is an undesired effect. Nonetheless, 20 mT was sufficient to achieve a satisfactory minimum

preferential magnetization index as high as 0.92. The effect of shear rate was also investigated (Figure S4 Supporting Information). As the nozzle size decreases, the shear forces acting on the extruded ink increase.^[22] Out of the sizes offered by the manufacturer, apart from the 1.2 mm nozzle used in the manuscript, another 0.84 mm nozzle was considered. The extruded magnetic ink experiences a 43% higher shear rate when extruded through the 0.84 mm nozzle as compared to 1.2 mm nozzle. A significant difference in magnetization programming efficiency could not be observed for the 0.84 mm nozzle with respect to the 1.2 mm nozzle despite the 43% higher shear rate. In order to further push the limits and evaluate the effects of even high shear forces, experiments were performed while considering a 0.58 mm nozzle. Unfortunately, printing with a smaller nozzle (0.58 mm) resulted in an uncontrollable extrusion process.

To negate the bias in the magnetic ink, an optional step of randomization was performed. The ink was remixed in the planetary mixer after the magnetization step and before printing. Despite introducing a bias, non-randomized ink proved more suitable for achieving preferential magnetization through orientation compared to randomized ink, as shown in Figure S2 (Supporting Information). Due to the process of planetary mixing during the randomization step, it is possible that the particles with opposite orientations came together and negated each other. This would not only reduce the overall magnetization of the material but also make it more difficult to orient the particles leading to a poorer preferential magnetization index. Eventually, this randomization step was skipped unless otherwise stated. It is worth underlining that neither the pre-magnetization nor the magnetic field-induced orientation step seems to hamper ink homogeneity or create particle agglomerates as can be seen from the Energy Dispersive X-Ray (EDX) images shown in Figure S3 (Supporting Information). The mechanical properties of the magnetic soft material are shown in Figure S5 (Supporting Information).

The effect of particle concentration on the orientation process was also investigated by varying the particle concentration by weight with respect to the resin in the magnetic ink (between 1.25:1, 1:1, and 0.75:1 particle: resin ratio). The preferential magnetization index in all three cases remained high for all directions – between 0.89 and 0.99. However, the absolute value of magnetization featured an increasing trend with increasing particle concentration. The average peak magnetizations observed were 41.67, 29.42, and 22.03 emu g⁻¹ for the particle concentrations of 1.25:1, 1:1, and 0.75:1, respectively. Ideally, the highest ratio of particles should be used to give the composite the strongest magnetic response. However, with increasing particle concentration, the risk of not fully curing the composite also comes into play. Increasing particle concentration challenges their dispersion in the ink, thus the homogeneity of the printed filament and printing outcomes overall.^[20] Therefore, while we demonstrated the feasibility of using a higher ratio of magnetic particles, we performed the additional experiments with 1:1 particle concentration by weight with respect to the resin. The standard deviation of preferential magnetization index stayed below 0.07 for all experiments, thereby showing low variability and high repeatability. The preferential magnetization indices from all characterization experiments

are tabulated in Supporting Information. In all the experiments getting a preferential magnetization index of 1, i.e., a 100% orientation in the desired direction was not possible. This could be ascribed to a few reasons. As described earlier, due to the magnetization step, there was a bias in the X-direction in the magnetic ink which was anyhow necessary for better efficiency. Second, as the extrusion process induces shear in the material, there could also be some shear alignment which resulted in the particles being aligned along the printing direction. Furthermore, errors might also derive from the characterization phase, as the samples were mounted manually on the VSM probes.

The orientation process was then employed to print magnetic structures for three actuation scenarios that require different magnetization profiles. A thin string twisting robot, a ribbon robot able to travel in narrow lumina, and a folding robot able to transport cargo were prototyped and tested.

A thin string robot that can twist under a remote rotating magnetic field can be used to induce a rotation at one of its ends. To achieve such a motion, a string robot (length 10 cm, diameter 1.2 mm) with magnetization which varied in a spiral fashion as shown in Figure 4 was printed (printing time ≈ 4 min). While the magnetization was always perpendicular to the long axis of the robot, its direction in that plane was varied in a circular fashion along its length. One end of the twisting robot was clamped to avoid rotating the entire string robot. A thin sheet of paper with an arrow drawn on it (referred to as a flag) was glued perpendicularly to the string robot at its free end to visualize the rotation generated at that end. When the robot was placed in a magnetic field generated by an External Permanent Magnet (EPM), the robot experienced an internal twist to try to align all the magnetic domains along the external magnetic field, thereby generating a rotation at the free end evidenced by the rotating flag. At this point, when the magnetic field (≈ 60 mT) rotated clockwise by rotating the EPM, the string robot twisted further to try to keep its net magnetization aligned with the external magnetic field (Figure 4B and Video S1, Supporting Information). The string robot twisted continuously following the direction of the magnetic field for two complete rotations. Once the EPM was taken away from the string robot causing a drop in the applied magnetic field, the elastic forces of the string robot made the robot snap back to its original shape one rotation at a time. Since the EPM also generates magnetic gradients, the robot was placed inside a tube during the experiments to prevent it from being pulled toward the magnet.

A ribbon robot able to bend in a sinusoidal wave pattern can be used to navigate narrow lumen, eventually inside the body. To achieve such a motion, a thin ribbon robot (length 23 mm, height 0.2 mm, and width 1.7 mm) with sine-wave magnetization was printed as depicted in Figure 5 (printing time ≈ 1 min). The magnetization profile is sinusoidal along the length of the ribbon robot while it remains the same along its width and thickness. Such a magnetization profile can induce travelling wave-like motions under a rotating magnetic field.^[16a] A straight 3 mm × 3 mm hollow tube was used to simulate a narrow lumen in the body. The ribbon robot was placed inside it and a magnetic field was applied using an EPM. Under the influence of a magnetic field, the robot took the shape of a sinusoidal wave. When the magnetic field was rotating, it created

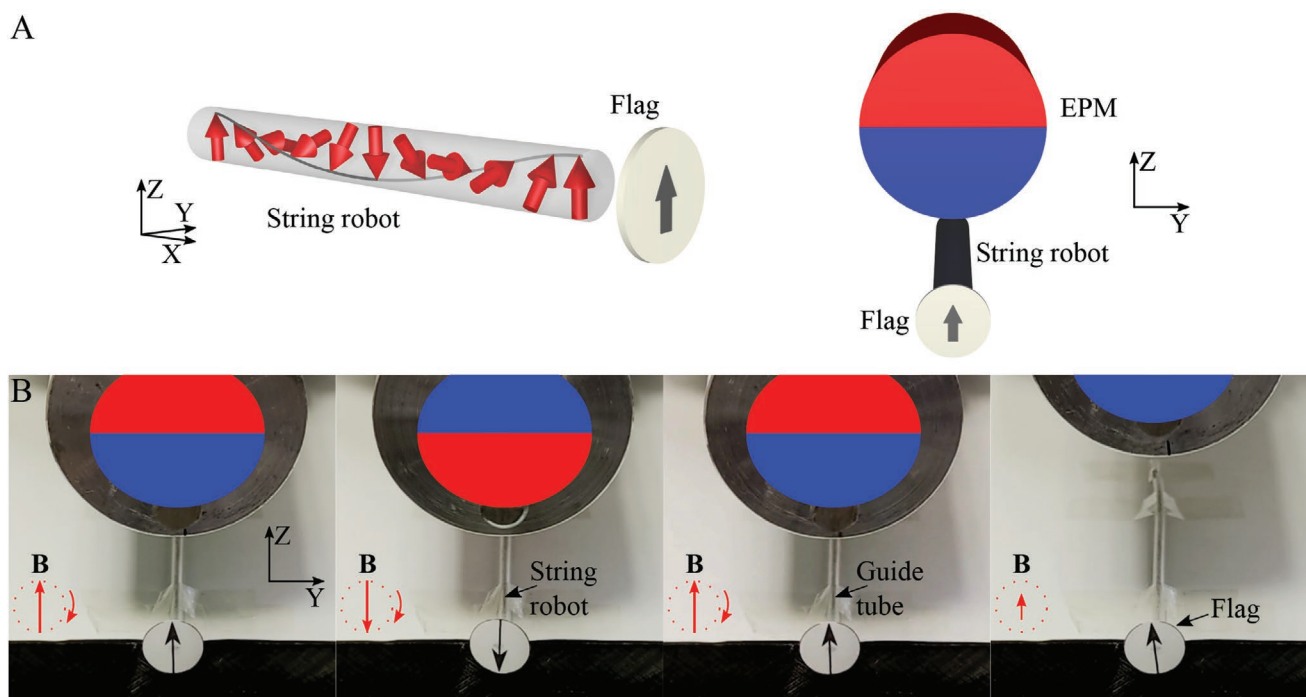


Figure 4. Twisting motion of a string robot under a rotating magnetic field. A) An exploded view showing the spiral magnetization profile of the robot, the flag attached to one end of it, and the position of the EPM placed above the robot such that their axes align. When the tips of arrows (representing the magnetization profile) are joined together, they form a spiral as shown. Drawing not to scale. B) (left to right) Twisting in the robot is indicated by the flag attached to it. The rotating magnetic field and twisting were both in a clockwise direction. The last frame shows the position of the flag after one of the snapbacks.

a travelling wave-like motion in the robot. Taking advantage of friction inside the narrow lumen, the travelling wave produced a translatory motion of the ribbon robot along the tube. An example of such a wave is shown in Figure 5B where, under a rotating magnetic field, the shape of the ribbon robot changed in a travelling-wave fashion (Video S2, Supporting Information). The translation speed thus achieved under a 0.67 Hz 40 mT rotating magnetic field was 0.53 mm s^{-1} corresponding to 0.023 bodylength per second. The translation speed not only depends on the rotational frequency of the external magnetic field but also on the friction inside the lumen. With an increase in friction, more traction can be achieved, and the translational speed can be increased.

A folding robot able to bend and close into the shape of a cube can be used to pick up, transport, and deliver cargoes to targeted locations. A thin sheet was printed (printing time $\approx 30 \text{ min}$) in the shape of a net of a cube (each square: $10 \text{ mm} \times 10 \text{ mm}$, thickness: 0.2 mm) where each section of the net folds to become one face of the emerging cube (Figure 6). When an external magnetic field (120 mT) perpendicular to the sheet was applied, each section of the net oriented itself to align its magnetization along the external magnetic field as seen in Figure 6C. Due to the programmed anisotropy in the 2D structure, it morphed into a cube-like 3D structure upon application of an external magnetic field making it suitable for pick and place tasks. Further, the magnetic field around a single permanent magnet is neither uniform in intensity nor in direction. Therefore, the face of the cube farthest from the magnet does not close fully. This resulted in an open cube which is taken

advantage of in picking up objects. To close this face, either the open cube was rolled so that reaction forces from the surface closed the face, or the EPM was brought closer to that face so that magnetic interaction aligned it in the right direction. The cube can be finally rolled by rotating the remote magnetic field.

Depending on the location of the object, the cube can be transported there and rolled over the object with the open face allowing the object to enter the cube. The cube can now be rolled back to pick up the object which stays within the cube. After pick-up, rolling the open cube in the direction of the open face closed the cube due to the reaction forces from the surface on which the cube is rolling. Utilizing the rolling motion, the object was transported to a desired location (Figure 6D). Once at the desired location, the cube was opened by removing the remote magnetic field which resulted in the object lying on top of the flat sheet. The external magnetic field was now applied in the opposite direction so that the cube folded inside out thereby lifting the object. At this stage, the magnetic field direction was tilted slightly to bend the cube and release the object (Figure 6E). Once the object was released, the cube was rolled back to its original position or to any other desired location (Figure 6F). This sequence of events can be seen in Video S3 (Supporting Information).

Each of the demonstrated magnetization profiles can also be produced using other existing methods in the literature. The twisting robot could also be produced using the method described by Zhang et. al.,^[16e] that requires a labor-intensive hand-assembly process of aligned magnetic domains called voxels, while the proposed method is neither labor-intensive

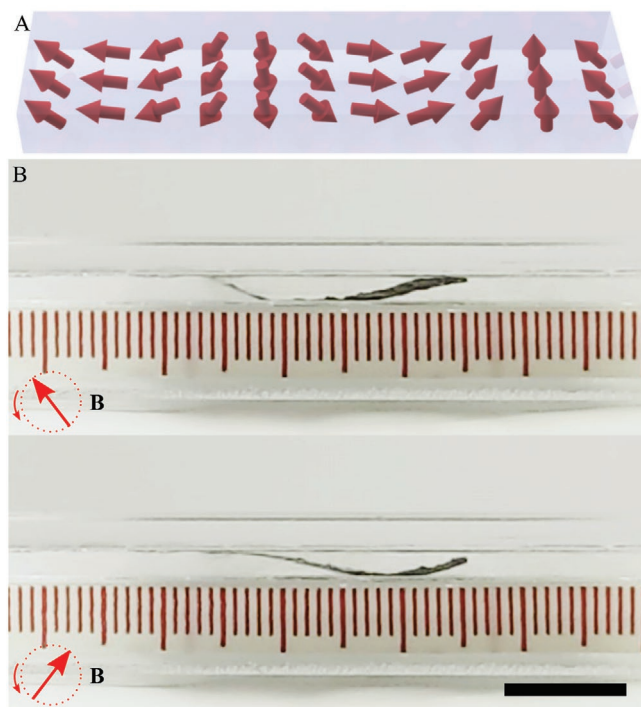


Figure 5. Travelling wave motion of a ribbon robot. A) A representation of the sinusoidal magnetization profile in the robot. The orientation of particles is represented by red arrows. Drawing not to scale. B) Travelling wave-like motion was observed within the robot under an anti-clockwise rotating magnetic field. Within a confined space, this motion was used to induce translation. Scale bar: 10 mm.

nor time-consuming. While the ribbon robot has been shown by Hu et al.,^[16a] the sinusoidal profile obtained there is through the jig-dependent process. Here, the sinusoidal profile is directly printed into the structure thereby eliminating the need to have an additional magnetization step in the jig for every robot. Though the cube robot could be produced using the method described by Diller et al.,^[16b] it would be a slow process achieving each direction individually and one after the other. The “voxelated” method to fabricate an earthworm-mimicking magnetic robot described by Zhang et al. can produce soft robots with magnetization profiles unachievable through other state-of-the-art 3D printing methods.^[16e] While it is envisioned that our 3D printing method can be used to fabricate even such complex magnetic soft robots, this paper focuses on establishing the feasibility of the approach by demonstrating exemplary small-scale soft robots with varied magnetization profiles.

3. Conclusion

In this paper, a novel way of incorporating magnetic anisotropy in soft structures is demonstrated. A printable magnetic ink was formulated consisting of a UV curable resin and magnetic particles and was extruded using a modified commercial extrusion bioprinter. For orienting the magnetic moment of the particles in the ink during extrusion, a custom electromagnetic coil system was designed, assembled, and characterized. The duration for particle orientation was theoretically calculated

thus dictating the printing speeds. This orientation process was characterized in 6 fundamental directions confirming the ability to orient particles in any desired direction. It is shown that using 20 mT field for orientation with 1:1 particle-to-resin ratio in the magnetic ink produced a preferential magnetization index up to 0.99 in the printed structure. Higher particle concentrations, while showing similar preferential magnetization indices (0.91–0.99) offered higher preferential magnetization peaks because of the presence of more magnetic material. When no randomization step was done higher magnetization peaks were obtained compared to prints with a randomization step.

Several examples with different magnetic anisotropies demonstrated the versatility of the proposed approach. A string robot (printing time \approx 4 min) that twists and rotates, a ribbon robot (printing time \approx 1 min) that can translate in confined spaces under rotating magnetic field, and a cube robot (printing time \approx 30 min) that can pick up, transport, and drop cargo were demonstrated. The presented approach gives designers the option of maximally utilizing the benefits of 3D printing along with imparting omnidirectional magnetization profile in the printed object. The process was shown to be time-efficient and repeatable. Some elements requiring further research exist. First, after magnetization the magnetic ink becomes very viscous, thus requiring a high-extrusion pressure. This also formed a limit on the nozzle size (\approx 0.8 mm) below which a precise control on extrusion becomes prohibitively difficult with the bioprinter employed in this study. In fact, when a larger extrusion pressure was applied, the plastic syringe started bending instead of the material being extruded, compromising the 3D printing. Second, with each of the 3 EM coils being perpendicular to each other, the elimination of magnetic gradients was not possible. As a result, the printed material tended to get attracted toward the EM coils. This led to some distortion in the printed structure. A method to produce magnetic field without magnetic gradients could be advantageous, for example, an 8-coil system as reported by Kummer et al.^[23] Third, while UV curing is a fast process in thin layers (order of minutes), it may not fully cure thicker layers quickly. This may lead to loss of shape of the printed material. Nonetheless, with proper curing, the custom 3D printing system developed here offers the flexibility to produce 3D structures along with the flexibility to incorporate a wide range of desired anisotropies in the printed structure at the same time, despite not having 100% preferential magnetization.

4. Experimental Section

Materials: The polymer part of the magnetic composite ink is composed of a UV curable resin (365 nm, UV electro 225-1, Momentive, USA) and UV photoinitiator (Momentive, USA) in 10:1 ratio by weight (together called resin for simplicity). The magnetic ink is composed of this resin and 5 μ m NdFeB particles (MQP-15-7-20065, Magnequench, Germany) in desired proportions.

Preparation of the Magnetic Ink: The resin was weighed in a plastic container and degassed for 30 min under vacuum to remove any bubbles. The photoinitiator and magnetic powder were added to the container, the container was closed, and the components mixed using a planetary mixer (IGT SimplyMix, Netherlands) for 60 s. This type

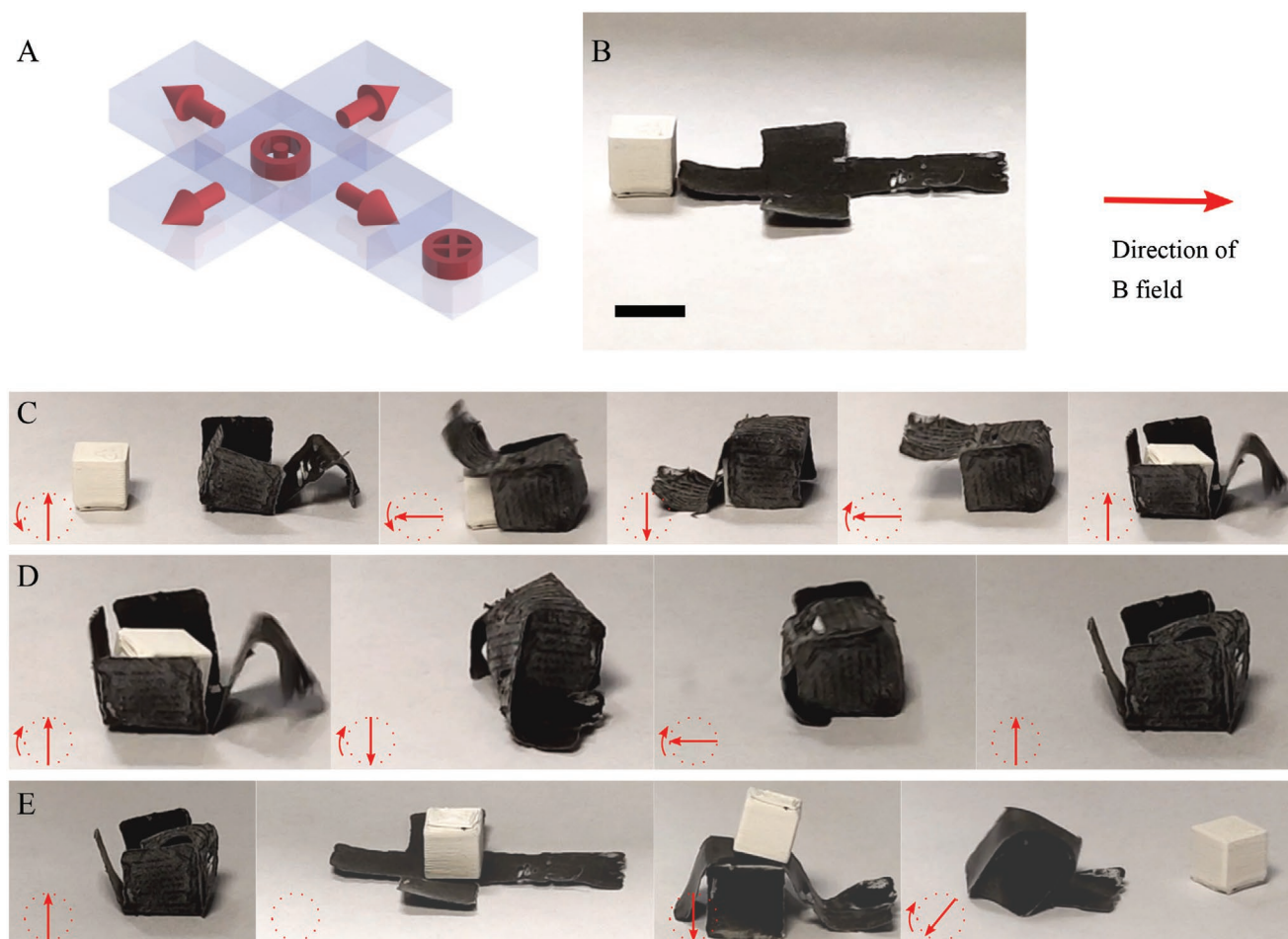


Figure 6. Loading, carrying, and dropping an object using a folding cube robot. A) A schematic of the printed sheet with six different magnetization directions on the six faces of the cube. Scale bar: 10 mm. B) The printed sheet with said magnetizations placed alongside a cubic object of 0.5 g. C) The cube folding under a magnetic field and rolling over the object to pick it up. D) The cube carrying the object to the desired location where E) it unfolds and drops the object at the target location before rolling back to a desired point.

of mixing is used for materials with a high viscosity such as pastes, paints, and slurries.^[24] This mixture was then transferred to a syringe and magnetized in an Impulse magnetizer (MAGNET-PHYSIK T-SERIES MF-AsA-ø25,0×60,0 mm-1218, Germany) at field greater than 2 T. Such a magnetization step magnetized all the particles in the syringe along its axis. To randomize the magnetized particles again, an additional planetary mixing step was optionally performed on this ink before printing. Once all the components were mixed, the ink was quite stable for a few hours after which, however, it started to cure rendering it unusable for printing. A particle concentration of 1:1 by weight with respect to the resin was used for all experiments unless otherwise mentioned.

UV Source: A high intensity (365 nm, 3500 mW cm⁻²) focused UV (Hamamatsu Lightningcure™ LC5, Japan) source was used to cure the extruded material.

The Electromagnetic Coils: The three electromagnetic coils which were orthogonal to each other were placed around the extruder such that the core of each coil was 5 mm away from the extrusion point. There were 480 windings of 1 mm diameter insulated copper wire in total in each coil, which were arranged in a stepped manner as can be seen in Figure 1B. The core was tapered and made of a soft magnetic material (Vacoflux-50, Vacuumschmelze, Germany). An orientation field of 20 mT was used unless otherwise mentioned. The currents in the coils were driven using Servo drives (Elmo Gold Solo Twitter, Israel) which were

in turn controlled using LabVIEW (V20.0f1, National Instruments, USA).

Measurement of Magnetic Fields: Magnetic fields were recorded using a TLE493D-W2B6 (Infineon, Germany) 3-axis magnetic sensor.

Measurement of Magnetization: The printed structures were characterized in a Vibrating Sample Magnetometer VSM (Microsense, EZ9, USA) to quantify their magnetization

Printing: A Dual Extrusion 3D Bioprinter (Omega, 3Dynamic, UK) was used, albeit only one extruder was utilized which uses 17HS4417 motors (ACT MOTOR, China). The 3D printer was in turn controlled either with Repetier Host (V2.1.6, Hot-World GmbH & Co. KG, Germany) or with LabVIEW (V20.0f1, National Instruments, USA). Commercially available 20 ml Leur Lock syringes (NORM-JECT®, HenkeSassWolf, Germany) and 1.2 mm nozzle (7018097, SmoothFlow tapered Tips, Nordson, USA) were used for extrusion. The printing speed was 25 mm min⁻¹ which is the lowest speed achievable with this printer. Having a low speed is important to give the particles enough time to reorient themselves in the desired direction.

Supporting Information

Supporting Information is available from the Wiley Online Library or from the author.

Acknowledgements

This work was supported by the ATLAS project. This project has received funding from the European Union's Horizon 2020 research and innovation programme under the Marie Skłodowska-Curie grant agreement No 813782.

Open Access Funding provided by Scuola Superiore Sant'Anna within the CRUI-CARE Agreement.

Conflict of Interest

The authors declare no conflict of interest.

Data Availability Statement

The data that support the findings of this study are available from the corresponding author upon reasonable request.

Keywords

3D printing, magnetic actuation, magnetic anisotropy, microrobotics, programmable magnetization, soft robots

Received: October 14, 2022

Revised: December 20, 2022

Published online: January 29, 2023

- [1] M. Zarek, M. Layani, I. Cooperstein, E. Sachyani, D. Cohn, S. Magdassi, *Adv. Mater.* **2016**, *28*, 4449.
- [2] M. Wehner, R. L. Truby, D. J. Fitzgerald, B. Mosadegh, G. M. Whitesides, J. A. Lewis, R. J. Wood, *Nature* **2016**, *536*, 451.
- [3] S. Fusco, M. S. Sakar, S. Kennedy, C. Peters, R. Bottani, F. Starsich, A. Mao, G. A. Sotiriou, S. Pané, S. E. Pratsinis, D. Mooney, B. J. Nelson, *Adv. Mater.* **2014**, *26*, 952.
- [4] D. Rus, M. T. Tolley, *Nature* **2015**, *521*, 467.
- [5] M. Sitti, *Nat. Rev. Mater.* **2018**, *3*, 74.
- [6] S. Felton, M. Tolley, E. Demaine, D. Rus, R. Wood, *Science* **2014**, *345*, 644.
- [7] C. Liu, Y. Tan, C. He, S. Ji, H. Xu, *Adv. Mater.* **2021**, *33*, 2105194.
- [8] R. M. Erb, J. S. Sander, R. Grisch, A. R. Studart, *Nat. Commun.* **2013**, *4*, 1712.
- [9] R. V. Martinez, C. R. Fish, X. Chen, G. M. Whitesides, *Adv. Funct. Mater.* **2012**, *22*, 1376.
- [10] a) Y. Kim, A. Parada German, S. Liu, X. Zhao, *Sci. Rob.* **2019**, *4*, eaax7329; b) G. Pittiglio, P. Lloyd, T. da Veiga, O. Onaizah, C. Pompili, J. H. Chandler, P. Valdastrì, *Soft Rob.* **2022**, *9*, 1120.
- [11] R. M. Erb, J. J. Martin, R. Soheilian, C. Pan, J. R. Barber, *Adv. Funct. Mater.* **2016**, *26*, 3859.
- [12] a) L. Hines, K. Petersen, G. Z. Lum, M. Sitti, *Adv. Mater.* **2017**, *29*, 1603483; b) I. Paprotny, S. Bergbreiter, presented at Small-Scale Robotics From Nano-to-Millimeter-Sized Robotic Systems and Applications, Karlsruhe, Germany, Vol. 8336, May **2014**.
- [13] J. Lussi, M. Mattmann, S. Sevim, F. Grigis, C. De Marco, C. Chautems, S. Pané, J. Puigmartí-Luis, Q. Boehler, B. J. Nelson, *Adv. Sci.* **2021**, *8*, 2101290.
- [14] Y. Zhang, M. Cong, D. Guo, D. Wang, *IEEE ASME Trans Mechatron* **2009**, *14*, 493.
- [15] a) V. Iacovacci, G. Lucarini, C. Innocenti, N. Comisso, P. Dario, L. Ricotti, A. Menciasci, *Biomed. Microdevices* **2015**, *17*, 112; b) B. Jiang, W. L. Hom, X. Chen, P. Yu, L. C. Pavelka, K. Kisslinger, J. B. Parise, S. R. Bhatia, R. B. Grubbs, *J. Am. Chem. Soc.* **2016**, *138*, 4616.
- [16] a) W. Hu, G. Z. Lum, M. Mastrangeli, M. Sitti, *Nature* **2018**, *554*, 81; b) T. Xu, J. Zhang, M. Salehizadeh, O. Onaizah, E. Diller, *Sci. Rob.* **2019**, *4*, eaav4494; c) H. Song, J. Spencer, A. Jander, J. Nielsen, J. Stasiak, V. Kasperchik, P. Dhagat, *J. Appl. Phys.* **2014**, *115*, 17E308; d) Y. Kim, H. Yuk, R. Zhao, S. A. Chester, X. Zhao, *Nature* **2018**, *558*, 274; e) J. Zhang, Z. Ren, W. Hu, R. H. Soon, I. C. Yasa, Z. Liu, M. Sitti, *Sci. Rob.* **2021**, *6*, eabf0112.
- [17] B. A. Praveena, N. Lokesh, A. Buradi, N. Santhosh, B. L. Praveena, R. Vignesh, *Mater Today Proc* **2022**, *52*, 1309.
- [18] J. Kim, S. E. Chung, S.-E. Choi, H. Lee, J. Kim, S. Kwon, *Nat. Mater.* **2011**, *10*, 747.
- [19] H. Deng, K. Sattari, Y. Xie, P. Liao, Z. Yan, J. Lin, *Nat. Commun.* **2020**, *11*, 6325.
- [20] C. Zhang, X. Li, L. Jiang, D. Tang, H. Xu, P. Zhao, J. Fu, Q. Zhou, Y. Chen, *Adv. Funct. Mater.* **2021**, *31*, 2102777.
- [21] L. Yang, N. Zhao, D. Liu, *Adv. Mech. Eng.* **2015**, *7*, <https://doi.org/10.1177/1687814015589686>.
- [22] J. R. Wagner, E. M. Mount, H. F. Giles, in *Extrusion*, 2nd ed. (Eds: J. R. Wagner, E. M. Mount, H. F. Giles), William Andrew Publishing, Oxford **2014**, p. 203.
- [23] M. P. Kummer, J. J. Abbott, B. E. Kratochvil, R. Borer, A. Sengul, B. J. Nelson, *IEEE Trans. Rob.* **2010**, *26*, 1006.
- [24] N. Adachi, M. Hashiba, O. Sakurada, *Ceram. Int.* **2004**, *30*, 1055.